A Computationally Efficient Beamforming Solution for Bistatic RF Sensing with RIS-Enhanced Target Illumination

Cengcang Zeng, *Student Member, IEEE,* Hongbin Li, *Fellow, IEEE*

***Abstract*— Reconfigurable intelligent surface (RIS) is gaining increasing interest for communications and sensing in urban/indoor environments, where line-of-sight (LOS) propagation is often obstructed by buildings, walls, and other RF-blocking objects. We consider a bistatic RF sensing system that employs RIS to provide enhanced target illumination and anti-blocking capabilities. The core problem is the joint design of the active transmit beamformer and the passive RIS beamformer, which is challenging due to non-convex constant modulus constraints on the latter. Conventional approaches typically resort to convex relaxation or direct optimization on the constant-modulus manifold, which are computationally intensive because of their iterative nature. By exploiting the geometric structures inherent in the problem, we derive an analytic solution in closed form. Additionally, we examine target detection with the RIS-assisted sensing system and quantitatively analyze the detection performance when the propagation paths in the system are subject to blocking. Finally, the RIS-assisted system is evaluated in various scenarios, including different RIS-sensor locations, channel estimation errors, and multi-path interference.**

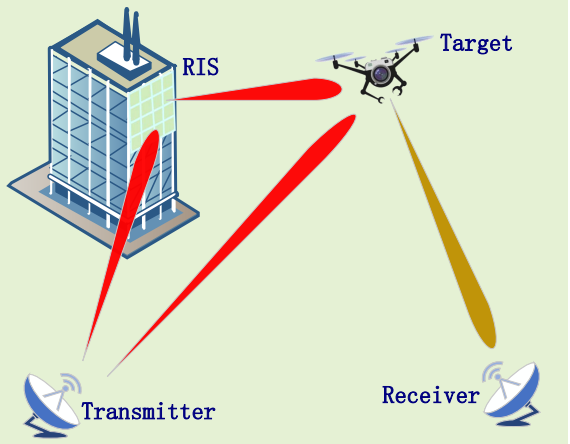

***Index Terms*— reconfigurable intelligent surface (RIS), non-line-of-sight (NLOS) RF sensing, beamforming, detection**

I. Introduction

CONVENTIONAL radio frequency (RF) sensing systems are heavily reliant on line-of-sight (LOS) paths, both from the transmitter (TX) to the target and from the target to the receiver (RX). However, in urban and indoor environments, the presence of obstacles such as walls, high-rise buildings, and mobility due to pedestrians and vehicles pose significant challenges to sensing functionality [1]. A conventional approach to dealing with non-line-of-sight (NLOS) targets is to deploy multiple TXs and RXs spread over the surveillance area, which effectively results in a distributed multi-input multi-output radar [2]. However, such a system is bulky, expensive to deploy and operate, and environmentally unfriendly because it employs multiple TXs that may create excessive RF emission.

In recent years, reconfigurable intelligent surface (RIS) has attracted much attention as a green and economic solution for NLOS communications and RF sensing. Specifically, RIS offers new ways to program and customize the wireless environment, which can greatly benefit next-generation wireless systems [3], [4]. Among various enabling signal processing techniques, joint active and passive beamforming is crucial in RIS-aided wireless systems [5]. Beyond terrestrial wireless communications, recent advances have explored the application of RIS in satellite-terrestrial networks [6]–[8] and simultaneous wireless information and power transfer (SWIPT) [9].

In RF sensing, a range of RIS-assisted solutions have been reported, covering various subjects from target detection [10]–[14], positioning [15], [16], joint detection and localization [17], to parameter estimation [18], [19]. In cluttered environments, RIS offers new ways for effective clutter suppression [20]–[22]. As the sensor, RIS, and target are spatially separated, an RIS-assisted sensing system is inherently distributed. Consequently, the sensing signals propagating through different paths may arrive at the sensor asynchronously, in particular when the system is used to cover a large surveillance area. The effects of and methods to deal with asynchronous propagation in RIS-assisted RF sensing were investigated in [23]. Meanwhile, RIS has also shown great potential for integrated sensing and communication (ISAC) [24]–[31].

This paper considers an RIS-assisted bistatic RF sensing system. The system is motivated by the need to offer NLOS RF sensing capabilities in urban and indoor environments. Specifically, the TX is envisioned as a base station offering

This work was supported in part by the National Science Foundation under grants CCF-2316865, ECCS-1923739, ECCS-2212940, and ECCS-2332534.

C. Zeng, and H. Li are with the Department of Electrical and Computer Engineering, Stevens Institute of Technology, Hoboken, NJ 07030 USA (e-mail: czeng2@stevens.edu; hli@stevens.edu).

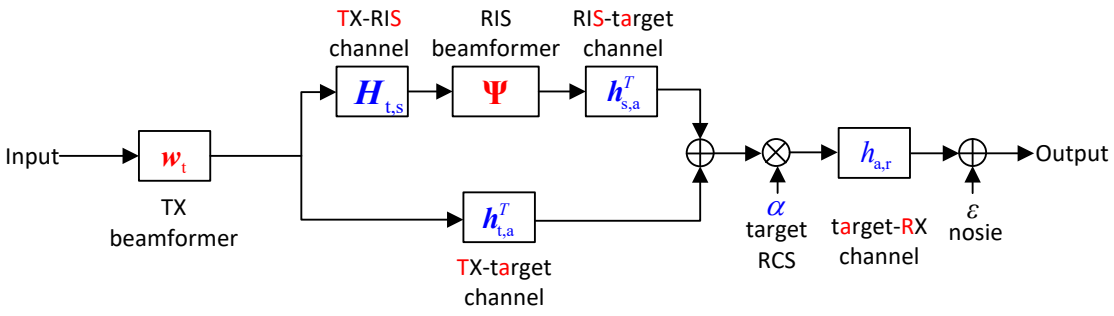

Fig. 1. Block diagram and symbols for the RIS-assisted bistatic system.

RF sensing service to a mobile user, acting as the RX. Due to the user's mobility, an RIS is employed to assist target illumination and enhance the system's ability to cope with blocking.

We address two related problems for the RIS-aided RF sensing system. The first is the joint design of the TX beamformer and the RIS beamformer. The problem is non-convex due to the constant modulus constraints on the phase shifters of the passive RIS beamformer. A conventional approach to such problems is based on semidefinite relaxation (SDR) (e.g., [11], [20], [32]), which lifts the problem to a high-dimensional space and thus incurs a significant penalty in complexity. A considerably more efficient alternative without lifting is based on direct optimization on the constant modulus manifold [33]. However, the method is an iterative algorithm that, for each iteration, requires several matrix-vector operations, including gradient calculation, projection to the tangent space of the manifold, gradient descent, and retraction of the resulting update to the manifold [34], thus still involving a high complexity. By leveraging inherent geometric structures of the problem, we present a closed-form solution to the joint beamforming problem, reducing the complexity by several orders of magnitude compared to the manifold optimization method. Our second problem is to study the impact of blocking on the RIS-assisted sensing system. We provide an analytical and quantitative analysis of the target detection performance in terms of the probability of false alarm and probability of detection in the presence of blocking. Furthermore, numerical results are presented to verify our theoretical analysis and examine the effects of varying RIS positions, channel estimation errors, obstacles in the direct or indirect target path, and multi-path interference.

In summary, the key contributions of our work include the following:

- A closed-form solution for the joint beamforming problem, with significantly reduced computational complexity compared with conventional convex relaxation or manifold optimization methods.
- A target detector for the RIS-assisted RF sensing system, based on the generalized likelihood ratio test principle.
- A detailed analysis of the impact of blocking on the target detection performance of the RIS-assisted system.

The remainder is organized as follows. The signal model for the RIS-assisted bistatic RF sensing system is introduced in Section II. Our proposed joint beamforming design is presented in Section III. Target detection and statistical analysis are discussed in Section IV. Section V contains numerical results, followed by conclusions in Section VI.

Notations: We use boldface symbols for vectors (lower case) and matrices (upper case). $(\cdot)^T$ denotes the transpose, $(\cdot)^*$ denotes the complex conjugate and $(\cdot)^H$ the conjugate transpose. $\|\cdot\|$ and $|\cdot|$ denote the vector 2-norm and absolute value, respectively. $\mathcal{CN}(m,\sigma^2)$ denotes the circularly symmetric complex Gaussian distribution with mean m and variance σ^2. $[\boldsymbol{X}]_{m,m}$ indicates the (m,m)-th element of matrix $\boldsymbol{X}$.

II. System Description and Problem Statement

We consider a bistatic RIS-assisted sensing system with an RIS installed to assist target illumination. The TX is a base station equipped with N_t antennas and the RX is a mobile user with a single antenna. The RIS comprises M passive reflecting elements. We use $\psi_m \in [0, 2\pi)$ to represent the phase shift associated with the m-th element of the RIS. The diagonal phase shifting matrix for the RIS is denoted by

$$\boldsymbol{\Psi} \triangleq \mathrm{diag}(e^{j\psi_1}, \cdots, e^{j\psi_M}). \tag{1}$$

After matched filtering and sampling, the received signal at the receiver can be represented as [10], [11]:

$$z = \alpha\sqrt{P_\mathrm{t}} h_{\mathrm{a,r}} (\boldsymbol{h}_{\mathrm{t,a}}^T + \boldsymbol{h}_{\mathrm{s,a}}^T \boldsymbol{\Psi} \boldsymbol{H}_{\mathrm{t,s}}) \boldsymbol{w}_\mathrm{t} + \epsilon, \tag{2}$$

where α the unknown complex amplitude of the target, P_t the total radar transmit power, while $\boldsymbol{h}_{\mathrm{t,a}} \in \mathbb{C}^{N_\mathrm{t}\times 1}$, $\boldsymbol{h}_{\mathrm{s,a}} \in \mathbb{C}^{M\times 1}$, $\boldsymbol{H}_{\mathrm{t,s}} \in \mathbb{C}^{M\times N_\mathrm{t}}$, and $h_{\mathrm{a,r}}$ denote the TX-target, RIS-target, TX-RIS, and target-RX channels, respectively (resp.). The vector $\boldsymbol{w}_\mathrm{t} \in \mathbb{C}^{N_\mathrm{t}\times 1}$ represents the TX beamforming vector, and ϵ denotes the noise, which has a zero mean and variance σ_n^2.

As shown in Fig. 1, the system comprises both cascade and parallel connections of several one-hop sub-channels $\boldsymbol{h}_{\mathrm{t,a}}$, $h_{\mathrm{a,r}}$, $\boldsymbol{H}_{\mathrm{t,s}}$, and $\boldsymbol{h}_{\mathrm{s,a}}$, which can be represented as [10], [11]:

$$\boldsymbol{h}_{\mathrm{t,a}} = \rho_{\mathrm{t,a}} \boldsymbol{a}_\mathrm{t}^*(\boldsymbol{\theta}_{\mathrm{t,a}}), \tag{3}$$

$$h_{\mathrm{a,r}} = \rho_{\mathrm{a,r}}, \tag{4}$$

$$\boldsymbol{H}_{\mathrm{t,s}} = \rho_{\mathrm{t,s}} \boldsymbol{a}_\mathrm{s}(\boldsymbol{\phi}_{\mathrm{t,s}}) \boldsymbol{a}_\mathrm{t}^H(\boldsymbol{\theta}_{\mathrm{t,s}}), \tag{5}$$

$$\boldsymbol{h}_{\mathrm{s,a}} = \rho_{\mathrm{s,a}} \boldsymbol{a}_\mathrm{s}^*(\boldsymbol{\theta}_{\mathrm{s,a}}), \tag{6}$$

where $\boldsymbol{a}_\mathrm{t}(\boldsymbol{\theta})$ represents the TX steering vector, which is a function of the relative transmit-receive location parameter

$\boldsymbol{\theta}$ that includes the aspect (azimuth/elevation) angles for far-field channels, or both the range and aspect angles for near-field channels. Similarly, $\boldsymbol{a}_{\rm s}(\boldsymbol{\phi})$ and $\boldsymbol{a}_{\rm s}(\boldsymbol{\theta})$ denotes the RIS steering vector with angles of arrival $\boldsymbol{\phi}$ and angles of departure $\boldsymbol{\theta}$, respectively. The complex-valued channel coefficients $\rho_{\rm t,a}$, $\rho_{\rm a,r}$, $\rho_{\rm t,s}$ and $\rho_{\rm s,a}$ are dependent on the antena gain (or RIS element area) and propagation distance. See, e.g., [10], [11], for additional details of the channel model.

The problem of interest is to jointly design the TX beamformer $\boldsymbol{w}_{\rm t}$ and RIS beamformer $\boldsymbol{\Psi}$ with a transmit power constraint on $\boldsymbol{w}_{\rm t}$ and constant modulus constraints on the diagonal elements of the diagonal RIS beamformer $\boldsymbol{\Psi}$. We will present solutions to the problem assuming knowledge of the channels except for the target amplitude, and assess performance in the presence of channel estimation errors.

III. Joint Beamforming Design

In this section, we address a joint beamforming design problem aimed at maximizing the received signal power

$$\gamma = P_{\rm t}\left|\alpha h_{\rm a,r}(\boldsymbol{h}_{\rm t,a}^T + \boldsymbol{h}_{\rm s,a}^T\boldsymbol{\Psi}\boldsymbol{H}_{\rm t,s})\boldsymbol{w}_{\rm t}\right|^2. \tag{7}$$

Specifically, the problem involves selecting the TX beamformer $\boldsymbol{w}_{\rm t}$ and the RIS phase matrix $\boldsymbol{\Psi}$ to optimize the power of the received signal, namely,

$$\begin{aligned}\max_{\boldsymbol{w}_{\rm t},\boldsymbol{\Psi}} \quad & \left|\alpha h_{\rm a,r}(\boldsymbol{h}_{\rm t,a}^T + \boldsymbol{h}_{\rm s,a}^T\boldsymbol{\Psi}\boldsymbol{H}_{\rm t,s})\boldsymbol{w}_{\rm t}\right|^2 \\ \text{s.t.} \quad & \|\boldsymbol{w}_{\rm t}\|^2 = 1 \\ & \boldsymbol{\Psi} = \text{diag}(e^{j\psi_1},\cdots,e^{j\psi_M}),\end{aligned} \tag{8}$$

where the constraint $\|\boldsymbol{w}_{\rm t}\|^2 = 1$ ensures the total transmit power is $P_{\rm t}$.

For any phase matrix $\boldsymbol{\Psi}$, it can be shown that the optimal transmit beamformer $\boldsymbol{w}_{\rm t}$ is given by the maximum ratio transmission (MRT) solution

$$\boldsymbol{w}_{\rm t}^\star = \frac{(\boldsymbol{h}_{\rm t,a}^T + \boldsymbol{h}_{\rm s,a}^T\boldsymbol{\Psi}\boldsymbol{H}_{\rm t,s})^H}{\|\boldsymbol{h}_{\rm t,a}^T + \boldsymbol{h}_{\rm s,a}^T\boldsymbol{\Psi}\boldsymbol{H}_{\rm t,s}\|}. \tag{9}$$

By substituting $\boldsymbol{w}_{\rm t}^\star$ into (8), the problem becomes

$$\begin{aligned}\max_{\boldsymbol{\Psi}} \quad & \left\|\boldsymbol{h}_{\rm t,a}^T + \boldsymbol{h}_{\rm s,a}^T\boldsymbol{\Psi}\boldsymbol{H}_{\rm t,s}\right\|^2 \\ \text{s.t.} \quad & \boldsymbol{\Psi} = \text{diag}(e^{j\psi_1},\cdots,e^{j\psi_M}).\end{aligned} \tag{10}$$

Problem (10) is non-convex due to the constant modulus constraints

$$|\boldsymbol{\Psi}_{m,m}| = 1, \quad m = 1,\ldots,M. \tag{11}$$

A standard approach to solving such problems is convex relaxation. Specifically, by defining

$$\boldsymbol{\psi} = [e^{j\psi_1},\cdots,e^{j\psi_M}]^T, \tag{12}$$

$$\boldsymbol{\phi} = [\boldsymbol{\psi}^T, 1]^T, \tag{13}$$

the non-homogeneous quadratic objective function in (10) can be converted to a homogeneous one:

$$\left\|\boldsymbol{h}_{\rm t,a}^T + \boldsymbol{h}_{\rm s,a}^T\boldsymbol{\Psi}\boldsymbol{H}_{\rm t,s}\right\|^2 = \boldsymbol{\phi}^H\boldsymbol{B}\boldsymbol{\phi}, \tag{14}$$

where $\boldsymbol{B}$ is an $(M+1)\times(M+1)$ matrix given by

$$\boldsymbol{B} = \begin{bmatrix}\text{diag}^H(\boldsymbol{h}_{\rm s,a})\boldsymbol{H}_{\rm t,s}^*\boldsymbol{H}_{\rm t,s}^T\,\text{diag}(\boldsymbol{h}_{\rm s,a}) & \text{diag}^H(\boldsymbol{h}_{\rm s,a})\boldsymbol{H}_{\rm t,s}^*\boldsymbol{h}_{\rm t,a} \\ \boldsymbol{h}_{\rm t,a}^H\boldsymbol{H}_{\rm t,s}^T\,\text{diag}(\boldsymbol{h}_{\rm s,a}) & \boldsymbol{h}_{\rm t,a}^H\boldsymbol{h}_{\rm t,a}\end{bmatrix}.$$

By introducing a rank-1 matrix $\boldsymbol{\Phi} = \boldsymbol{\phi}\boldsymbol{\phi}^H$ and neglecting its rank structure, (10) can be relaxed into a semidefinite relaxation (SDR) problem

$$\begin{aligned}\max_{\boldsymbol{\Phi}} \quad & \text{tr}(\boldsymbol{\Phi}\boldsymbol{B}) \\ \text{s.t.} \quad & |\boldsymbol{\Phi}_{m,m}| = 1, m = 1,\ldots,M, \\ & \boldsymbol{\Phi}_{M+1,M+1} = 1,\end{aligned} \tag{15}$$

which is convex and readily solvable by an off-shelve solver. Finally, a feasible solution $\boldsymbol{\psi}$ can be recovered from the convex solution $\boldsymbol{\Phi}$ via randomization (see, e.g., [20], [32]).

The above SDR solution lifts the M-dimensional problem (10) to an $(M+1)^2$-dimensional problem (15), leading to a significant complexity penalty. A more efficient solution without lifting is based on direct optimization on manifold [33]. Specifically, problem (10) is a quadratic maximization on the *complex circle manifold*

$$\mathcal{S}^M \triangleq \{\boldsymbol{\psi}\in\mathbb{C}^M : |\boldsymbol{\psi}_m| = 1, m = 1,\ldots,M\}, \tag{16}$$

where $\mathbb{C}^M$ denotes the M-dimensional complex space. Therefore, (10) can be solved by iterative gradient descent on $\mathcal{S}^M$, which employs a projection of the conventional gradient of the objective function to the tangent space of $\mathcal{S}^M$. The manifold gradient descent approach is not only much simpler but also offers notably better performance than its SDR counterpart [34]. Each iteration of the manifold gradient descent approach consists of a gradient calculation, projecting the gradient to the tangent space, a gradient descent on the tangent space, and a retraction of the resulting update to $\mathcal{S}^M$, which involves matrix/vector operations. Therefore, the associated complexity is still high, especially when M is large.

In the following, we derive a closed-form solution to (10) by exploiting its inherent geometric structures. We start by rewriting the objective function as [cf. (5)]

$$\left\|\boldsymbol{h}_{\rm t,a}^T + \boldsymbol{h}_{\rm s,a}^T\boldsymbol{\Psi}\boldsymbol{H}_{\rm t,s}\right\|^2 = \left\|\boldsymbol{h}_{\rm t,a}^T + \rho_{\rm t,s}\rho_{\rm s,a}\boldsymbol{\psi}^T\boldsymbol{s}\boldsymbol{a}_{\rm t}^H(\boldsymbol{\theta}_{\rm t,s})\right\|^2, \tag{17}$$

where

$$\boldsymbol{s} \triangleq \boldsymbol{a}_{\rm s}^*(\boldsymbol{\theta}_{\rm s,a}) \odot \boldsymbol{a}_{\rm s}(\boldsymbol{\phi}_{\rm t,s}), \tag{18}$$

with $\odot$ denoting the Hadamard product. Note that (17) involves a sum of two vectors, namely $\boldsymbol{h}_{\rm t,a}^T$ and a scaled version of $\boldsymbol{a}_{\rm t}^H(\boldsymbol{\theta}_{\rm t,s})$, which are in general linearly independent of each other. To maximize (17), we take the following steps. Firstly, we make the magnitude of the second vector $\rho_{\rm t,s}\rho_{\rm s,a}\boldsymbol{\psi}^T\boldsymbol{s}\boldsymbol{a}_{\rm t}^H(\boldsymbol{\theta}_{\rm t,s})$ as large as possible, and secondly, make the inner product of the two vectors as large as possible. To this end, we write

$$\boldsymbol{\psi} = e^{\jmath\bar{\xi}}\bar{\boldsymbol{\psi}}. \tag{19}$$

The first step involves the following sub-optimization problem

$$\begin{aligned}\max_{\bar{\boldsymbol{\psi}}} \quad & |\bar{\boldsymbol{\psi}}^T\boldsymbol{s}| \\ \text{s.t.} \quad & \bar{\boldsymbol{\psi}} = [e^{j\bar{\psi}_1},\cdots,e^{j\bar{\psi}_M}]^T.\end{aligned} \tag{20}$$

It can be readily verified that the optimum $\bar{\psi}$ is given by

$$\bar{\boldsymbol{\psi}}^{\star} = [e^{-j\angle s_1}, \cdots, e^{-j\angle s_M}]^T, \tag{21}$$

where $\angle x$ represents the phase of the complex number x and s_m signifies the m-th entry of $\boldsymbol{s}$. Note that the above solution makes $\bar{\boldsymbol{\psi}}^{\star T}\boldsymbol{s}$ a real and non-negative number.

For the second step, we note that (17) becomes

$$\|\boldsymbol{h}_{\mathrm{t,a}}^T + e^{j\bar{\varsigma}}\widetilde{\boldsymbol{a}}_{\mathrm{t}}^H(\boldsymbol{\theta}_{\mathrm{t,s}})\|^2, \tag{22}$$

where

$$\widetilde{\boldsymbol{a}}_{\mathrm{t}}(\boldsymbol{\theta}_{\mathrm{t,s}}) = \rho_{\mathrm{t,s}}\rho_{\mathrm{s,a}}\boldsymbol{a}_{\mathrm{t}}(\boldsymbol{\theta}_{\mathrm{t,s}})\boldsymbol{s}^H\bar{\boldsymbol{\psi}}^{\star}. \tag{23}$$

Clearly, the problem reduces to the following inner product maximization:

$$\bar{\varsigma}^{\star} = \arg\ \max_{\bar{\varsigma}} \Re\{e^{j\bar{\varsigma}}\widetilde{\boldsymbol{a}}_{\mathrm{t}}^H(\boldsymbol{\theta}_{\mathrm{t,s}})\boldsymbol{h}_{\mathrm{t,a}}^*\}, \tag{24}$$

where $\Re\{\cdot\}$ takes the real part of the argument. The solution is given by

$$\begin{aligned}\bar{\varsigma} &= -\angle\left(\widetilde{\boldsymbol{a}}_{\mathrm{t}}^H(\boldsymbol{\theta}_{\mathrm{t,s}})\boldsymbol{h}_{\mathrm{t,a}}^*\right)\\ &= -\angle\left(\bar{\boldsymbol{\psi}}^{\star T}\rho_{\mathrm{t,s}}\rho_{\mathrm{s,a}}\boldsymbol{s}\boldsymbol{a}_{\mathrm{t}}^H(\boldsymbol{\theta}_{\mathrm{t,s}})\boldsymbol{h}_{\mathrm{t,a}}^*\right)\\ &= -\angle\left(\rho_{\mathrm{t,s}}\rho_{\mathrm{s,a}}\boldsymbol{a}_{\mathrm{t}}^H(\boldsymbol{\theta}_{\mathrm{t,s}})\boldsymbol{h}_{\mathrm{t,a}}^*\right),\end{aligned} \tag{25}$$

where in the second equality, we dropped $\bar{\boldsymbol{\psi}}^{\star T}\boldsymbol{s}$ because it is real and non-negative. Finally, the optimal diagonal phase shift matrix is given by

$$\boldsymbol{\Psi}^{\star} = e^{j\bar{\varsigma}^{\star}}\mathrm{diag}(\bar{\boldsymbol{\psi}}^{\star}). \tag{26}$$

In summary, the proposed joint beamforming scheme consists of (9), (21), and (25), assuming that $\boldsymbol{h}_{\mathrm{t,a}}$, $\boldsymbol{H}_{\mathrm{t,s}}$, and $\boldsymbol{h}_{\mathrm{s,a}}$ are known. In practice, the channels are usually unknown and replaced by their estimates [35]. We will examine the impact of channel estimation errors in Section V.

Remark: In deriving the above joint beamforming scheme, it is implicitly assumed that only one target is present in the radar scene. However, our scheme can also be utilized for multi-target detection. Specifically, in standard radar operation, the surveillance area is divided into multiple *range cells*, with the cell size inversely proportional to the bandwidth of the radar waveform. Targets residing in different range cells are resolvable. For multi-target detection, the RIS-aided radar scans one range cell at a time by letting the radar TX beamformer and RIS beamformer collaboratively steer their beams toward that cell and decides if a target is present or not—the underlying detection problem is considered in Section IV. The process is repeated until all range cells have been scanned and all targets are detected. It is worth noting that for each interrogated cell, the collaborative transmit and RIS beams are determined by the proposed beamforming scheme, namely (9), (21), and (25).

IV. Target Detection

The surveillance environment in urban and indoor settings often contains numerous obstructive elements, e.g., walls and moving objects like pedestrians and vehicles. Such obstruction can block either the direct or indirect signal path. In the following, we consider the detection performance of the RIS sensing system without or with obstruction.

A. With No Obstruction

When both the direct and indirect paths are free of obstruction, (2) can be written as

$$z = \alpha(g_{\mathrm{d}} + g_{\mathrm{i}}) + \epsilon, \tag{27}$$

where

$$g_{\mathrm{d}} = \sqrt{P_{\mathrm{t}}}h_{\mathrm{a,r}}\boldsymbol{h}_{\mathrm{t,a}}^T\boldsymbol{w}_{\mathrm{t}} \tag{28}$$

denotes the equivalent channel of the direct path and

$$g_{\mathrm{i}} = \sqrt{P_{\mathrm{t}}}h_{\mathrm{a,r}}\boldsymbol{h}_{\mathrm{s,a}}^T\boldsymbol{\Psi}\boldsymbol{H}_{\mathrm{t,s}}\boldsymbol{w}_{\mathrm{t}} \tag{29}$$

denotes the equivalent channel of the indirect path. The target detection problem is described by the following hypothesis testing:

$$\text{target absent:} \qquad \mathcal{H}_0 : z = \epsilon, \tag{30a}$$

$$\text{target present:} \qquad \mathcal{H}_1 : z = \alpha(g_{\mathrm{d}} + g_{\mathrm{i}}) + \epsilon. \tag{30b}$$

It can be shown that the generalized likelihood ratio test, which uses the maximum likelihood estimate of the target amplitude α in the likelihood ratio test, for (30) is given by

$$T = |z| \underset{\mathcal{H}_0}{\overset{\mathcal{H}_1}{\gtrless}} \gamma. \tag{31}$$

Under $\mathcal{H}_1$, z is complex Gaussian with mean $\alpha(g_{\mathrm{d}} + g_{\mathrm{i}})$ and variance σ_n^2, i.e., $z \sim \mathcal{CN}\big(\alpha(g_{\mathrm{d}} + g_{\mathrm{i}}), \sigma_n^2\big)$, while under $\mathcal{H}_0$, $z \sim \mathcal{CN}(0, \sigma_n^2)$. Therefore, T is a Rayleigh distribution under $\mathcal{H}_0$ with probability density function (PDF) given by

$$p_T(t|\mathcal{H}_0) = \frac{2t}{\sigma_n^2}e^{-\frac{t^2}{\sigma_n^2}},\ t \geq 0. \tag{32}$$

and a Rice distribution under $\mathcal{H}_1$ given by

$$p_T(t|\mathcal{H}_1) = \frac{2t}{\sigma_n^2}e^{-\frac{1}{\sigma_n^2}(t^2+\beta^2)}I_0\Big(\frac{2\beta t}{\sigma_n^2}\Big),\ t \geq 0, \tag{33}$$

where $\beta^2 = \big|\alpha(g_{\mathrm{d}} + g_{\mathrm{i}})\big|^2$ and $I_0(\cdot)$ is the modified Bessel function of the first kind with order zero. It follows that the probability of false alarm P_f can be calculated as

$$P_f = \int_{\gamma}^{\infty} p_T(t|\mathcal{H}_0)dt = e^{\frac{-\gamma^2}{\sigma_n^2}}. \tag{34}$$

Then, the threshold for a given P_f is

$$\gamma = \sqrt{-\sigma_n^2 \ln P_f}. \tag{35}$$

Similarity, the probability of detection $P_d(g_{\mathrm{d}}, g_{\mathrm{i}})$, which depends on the direct and indirect channels g_{d} and g_{i}, can be expressed by using a generalized Marcum-Q function:

$$\begin{aligned}P_d(g_{\mathrm{d}}, g_{\mathrm{i}}) &= \int_{\gamma}^{\infty} p_T(t|\mathcal{H}_1)dt\\ &= Q_M\left(\frac{\sqrt{2}}{\sigma_n}|\alpha|^2\big|(g_{\mathrm{d}} + g_{\mathrm{i}})\big|^2, \frac{\sqrt{2}}{\sigma_n}\gamma\right).\end{aligned} \tag{36}$$

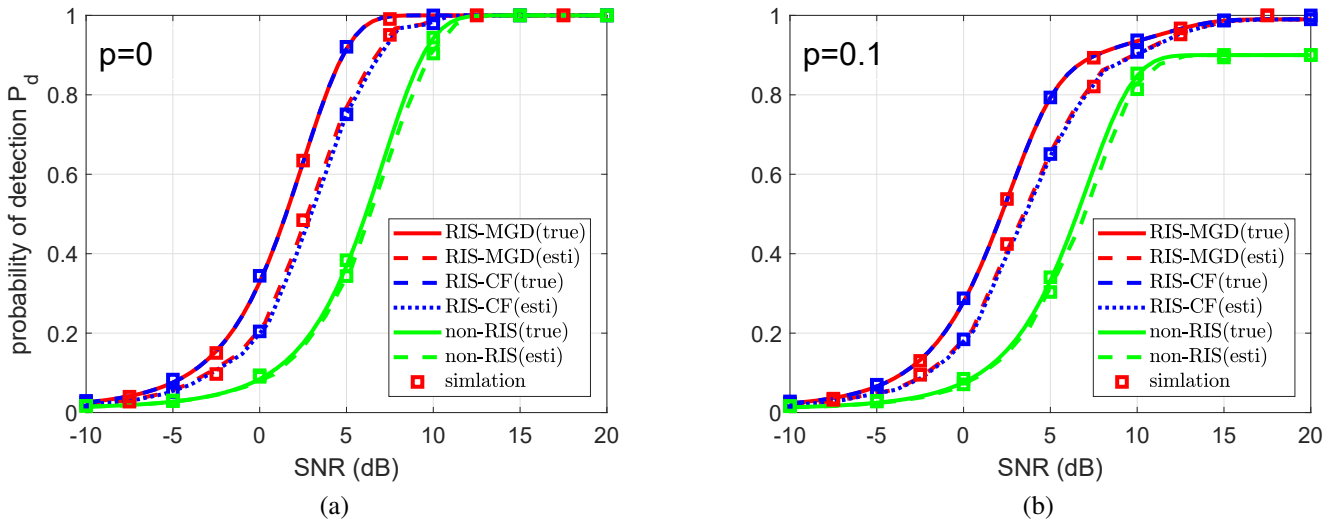

Fig. 2. Comparison of the RIS-MGD and RIS-CF schemes with the non-RIS scheme in Case 1 (RIS is close to RX), when using *true* channels and, respectively, *estimated* channels, assuming identical blocking probability $p = p_{\rm d} = p_{\rm i}$ for the direct and indirect paths. (a) $p = 0$, i.e., no blocking in either path. (b) $p = 0.1$.

B. With Random Obstruction

Suppose blocking may take place independently in the direct and indirect path. To model this phenomenon, we introduce a multiplicative binary random variable for each path, i.e., $b_{\rm d}$ for the direct path and $b_{\rm i}$ for the indirect path, which take value 1 (unblocked) and 0 (blocked). Then, the received signal under $\mathcal{H}_1$ is given by $z = \alpha(b_{\rm d}g_{\rm d} + b_{\rm i}g_{\rm i}) + \epsilon$. As blocking is random, the system designer does not know a priori if any path is blocked. Therefore, the detector takes the same form as (31). The average probability of detection that takes into account of random blocking is given by

$$\begin{aligned}\bar{P}_d =& p_{\rm d}p_{\rm i}P_d(0,0) + p_{\rm i}(1-p_{\rm d})P_d(g_{\rm d},0)\\ &+ p_{\rm d}(1-p_{\rm i})P_d(0,g_{\rm i})\\ &+ (1-p_{\rm d})(1-p_{\rm i})P_d(g_{\rm d},g_{\rm i}).\end{aligned} \tag{37}$$

where

$$p_{\rm d} = P(b_{\rm d} = 0), \tag{38}$$

$$p_{\rm i} = P(b_{\rm i} = 0) \tag{39}$$

denote the blocking probability of the direct and indirect path, respectively.

V. Numerical Results

While the proposed beamforming scheme was derived for single-path LOS channels, we examine its performance in both single-path and multi-path channels. In the following, we first discuss the simulation setup in Section V-A, and then Section V-B and Section V-C contain the numerical results in single-path and multi-path channels, respectively.

A. Simulation Setup

We compare the RIS-assisted system with a conventional bistatic phased-array radar, referred to as the **non-RIS** scheme for brevity, which is equipped with the same TX array as the former but without RIS. For the RIS system, we consider both the proposed solution in closed form, abbreviated as **RIS-CF**, and the one based on manifold gradient descent, denoted as **RIS-MGD**. The system parameters are similar to those of [10], with a carrier frequency 10 GHz, noise variance $\sigma_n^2 = -90$dBm, and target radar cross-section (RCS) of 0.02m^2. The TX array is a uniform linear array with $N_{\rm t} = 64$ antennas and a half-wavelength inter-element spacing, while the RX has a single antenna. The radar TX and RX and the target are located at: $(0, 0, 20)$m, $(-250, 1200, 2)$m, and $(-300, 1250, 20)$m, resp. Both systems share the same transmit power and noise variance. The SNR is defined as

$$\text{SNR} = P_{\rm t}\frac{|h_{\rm a,r}|^2\|\boldsymbol{h}_{\rm t,a}\|^2}{\sigma_n^2}. \tag{40}$$

The RIS is a uniform planar array of $M = 101\times101$ elements with half-wavelength spacing. To examine the impact of the RIS location, we consider *two cases*:

- Case 1: RIS is located at $(-500, 0, 10)$m, which is close to TX, and
- Case 2: RIS is located at $(-1000, 0, 10)$m, which is far from TX.

While the beamformers in Section II assumes knowledge of the channels, channel estimation needs to be performed in practice. To illustrate the impact of channel estimation errors, we include results obtained using both the *true* and *estimated* channels. The estimated channels contain an average estimation error of $\pm10\%$ for channel coefficients and $\pm25\%$ of the array mainbeam width for aspect angles [20].

B. Single-Path Channels

In our simulations, we first consider a setup where each channel has only one path, i.e., LOS path. Figs. 2(a) and 2(b) depict the probability of detection P_d versus SNR in Case 1, where the RIS is close to the TX with the probability of false alarm set to $P_f = 10^{-2}$. It is observed that the theoretical

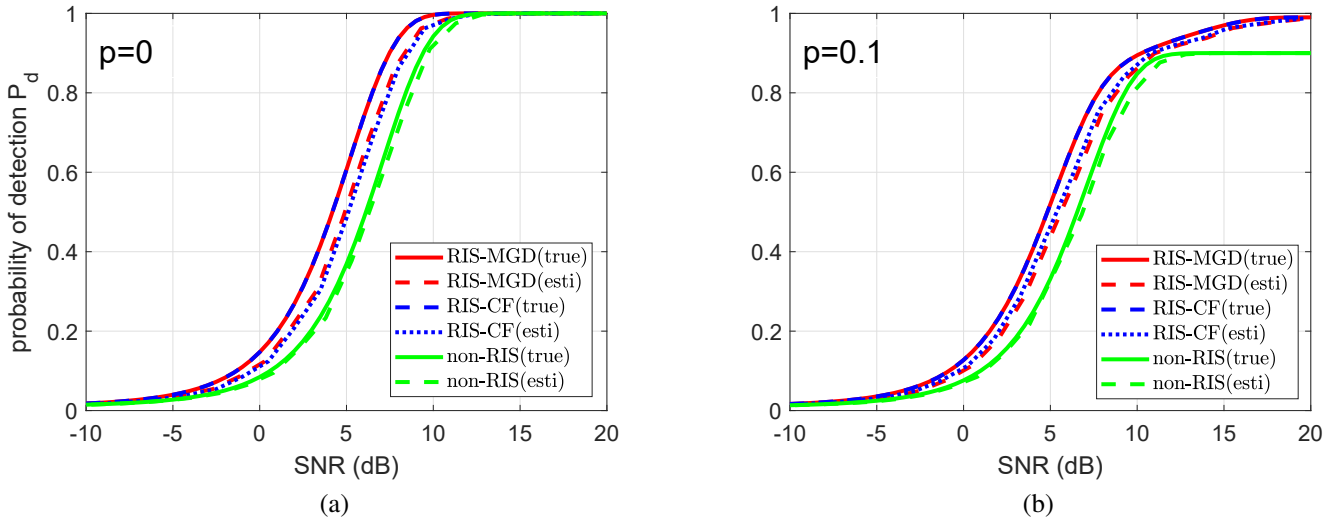

Fig. 3. Comparison of the RIS-MGD and RIS-CF schemes with the non-RIS scheme in Case 2 (RIS is far from RX), when using *true* channels and, respectively, *estimated* channels, assuming identical blocking probability $p = p_{\mathrm{d}} = p_{\mathrm{i}}$ for the direct and indirect paths. (a) $p = 0$, i.e., no blocking in either path. (b) $p = 0.1$.

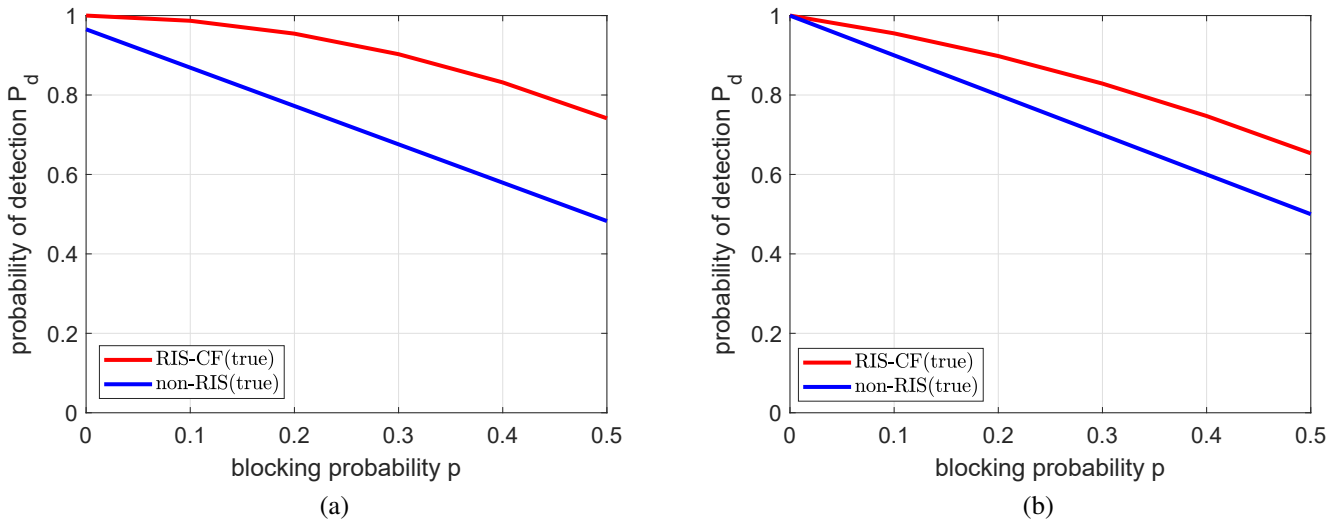

Fig. 4. The impact of different blocking probability when SNR $= 15$dB. (a) Case 1 where RIS is close to RX. (b) Case 2 where RIS is far from RX.

analysis in Section IV match the simulation results. When comparing the RIS and non-RIS schemes, RIS significantly improves the detection performance, regardless of whether there is obstruction. A comparison between Figs. 2(a) and 2(b) shows that, while obstruction degrades all schemes, RIS offers better resistance against obstruction than the non-RIS scheme. Notably, the non-RIS scheme exhibits an irreducible detection error floor that persists even with increasing SNR. These figures also reveal that channel estimation error inevitably degrades the performance of all systems. However, even with the substantial errors considered in these results, target detection can still benefit significantly from RIS.

Figs. 3(a) and 3(b) show the results for Case 2, where the RIS is positioned far from the TX, with the other simulation parameters kept the same as in the previous results. Although the relationships among the different methods are similar to those in in Figs. 2(a) and 2(b), we observe that, with a larger TX-RIS distance, the RIS schemes experience a performance loss. This is because the additional TX-RIS-target link leveraged by the RIS schemes form a cascade channel, with the overall channel gain that is the product of the channel gains associated with the TX-RIS link and RIS-target link, respectively. As the RIS moves farther from the TX, The cascade channel weakens, leading to a diminishing gain of the RIS schemes over the non-RIS scheme. Nevertheless, for the considered scenario, the RIS schemes with accurate channel information still outperform the non-RIS scheme by about 2 dB when there is no obstruction, as shown in Fig. 3(a); moreover, they are free of the error floor that the non-RIS scheme exhibits when obstruction is present. For the two RIS schemes, namely RIS-CF and RIS-MGD, we see from both Figs. 2 and 3 that they yield identical results with true channels and negligible differences with estimated channels. However, a comparison of their required floating-point operations (flops)

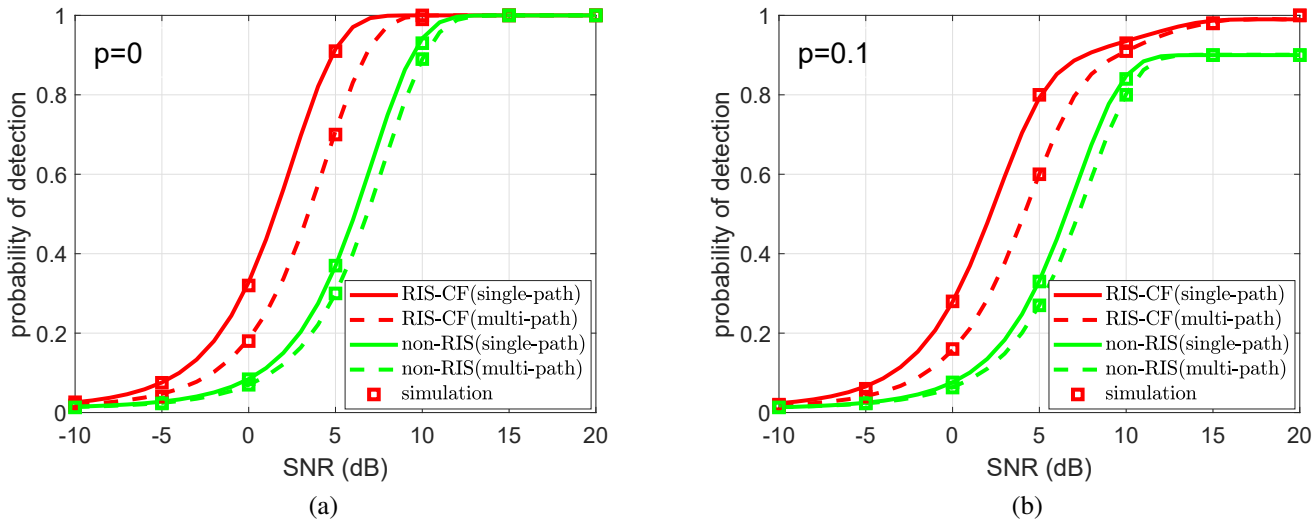

Fig. 5. The comparison between single-path and multi-path for Case 1 when SNR $= 15$dB. (a) $p = 0$. (b) $p = 0.1$.

indicates that, for the system parameters used in these examples, RIS-MGD requires about 2.5×10^8 flops to solve the joint design problem, while RIS-CF requires approximately 5.9×10^4 flops. The computational advantage of RIS-CF is especially beneficial in dynamic sensing environments (e.g., tracking a moving target), where the beamformers needs to be frequently updated.

To further investigate the impact of obstructions on detection capabilities, Fig. 4 demonstrates the correlation between P_d and the blocking probability at SNR $= 15$dB. It shows that as the blocking probability increases, both schemes are affected. However, the RIS scheme still significantly outperforms the non-RIS scheme across all values of the blocking probability.

C. Multi-Path Channels

In practical communication environments, a channel may consist of multiple paths, including one LOS path and several NLOS paths. Considering multi-path propagation caused by scatterers in the environment, the TX-target channel $\boldsymbol{h}_{\mathrm{t,a}}$, the TX-RIS channel $\boldsymbol{H}_{\mathrm{t,s}}$, and the RIS-target channel $\boldsymbol{h}_{\mathrm{s,a}}$ are modeled using the geometric Saleh-Valenzuela (SV) model [36], [37]:

$$\boldsymbol{h}_{\mathrm{t,a}} = \rho_{\mathrm{t,a},0}\boldsymbol{a}_{\mathrm{t}}^{*}(\boldsymbol{\theta}_{\mathrm{t,a},0}) + \sum_{l=1}^{L_{\mathrm{t,a}}-1} \rho_{\mathrm{t,a},l}\boldsymbol{a}_{\mathrm{t}}^{*}(\boldsymbol{\theta}_{\mathrm{t,a},l}) \tag{41}$$

$$\begin{aligned}\boldsymbol{H}_{\mathrm{t,s}} = {} & \rho_{\mathrm{t,s},0}\boldsymbol{a}_{\mathrm{s}}(\boldsymbol{\phi}_{\mathrm{t,s},0})\boldsymbol{a}_{\mathrm{t}}^{H}(\boldsymbol{\theta}_{\mathrm{t,s},0}) \\ & + \sum_{l=1}^{L_{\mathrm{t,s}}-1} \rho_{\mathrm{t,s},l}\boldsymbol{a}_{\mathrm{s}}(\boldsymbol{\phi}_{\mathrm{t,s},l})\boldsymbol{a}_{\mathrm{t}}^{H}(\boldsymbol{\theta}_{\mathrm{t,s},l}),\end{aligned} \tag{42}$$

$$\boldsymbol{h}_{\mathrm{s,a}} = \rho_{\mathrm{s,a},0}\boldsymbol{a}_{\mathrm{s}}^{*}(\boldsymbol{\theta}_{\mathrm{s,a},0}) + \sum_{l=1}^{L_{\mathrm{s,a}}-1} \rho_{\mathrm{s,a},l}\boldsymbol{a}_{\mathrm{s}}^{*}(\boldsymbol{\theta}_{\mathrm{s,a},l}), \tag{43}$$

where $L_{\mathrm{t,a}}$, $L_{\mathrm{t,s}}$, and $L_{\mathrm{s,a}}$ represent the number of paths for the TX-target, TX-RIS, and RIS-target channels, respectively. The channel coefficients $\rho_{\mathrm{t,a},l}$, $\rho_{\mathrm{t,s},l}$, and $\rho_{\mathrm{s,a},l}$ denote the complex gains of the l-th path, where when $l = 0$, it refers to the LOS path. The Rician factor $K \triangleq \frac{|\rho_0|^2}{\sum_{l=1}^{L-1}|\rho_l|^2}$ quantifies the ratio of energy in the LOS path to the total energy in all NLOS paths.

In the multi-path scenario, the received signal under hypothesis $\mathcal{H}_1$ is still given by (2), with the individual channels for the TX-target, TX-RIS, and RIS-target links defined in (41), (42), and (43). The RIS can be designed by using the proposed method discussed in Section III, which phase aligns only the LOS path, while neglecting the NLOS paths. The resulting detection performance is expected to be acceptable, as long as the LOS path is significantly stronger than the NLOS paths, which is typical in most wireless environments. In the following, we evaluate this approach both through theoretical calculation and computer simulation.

The detection performance in the multi-path scenario can be determined similarly to the single-path case. Specifically, under $\mathcal{H}_0$, the received signal consists only of noise, as described in (30a), so the false alarm probability P_f and the detection threshold γ remain unchanged, as defined by (34) and (35), respectively. In contrast, under $\mathcal{H}_1$, the received signal includes contributions from the target, resulting in a change in the received energy because of the presence of both LOS and NLOS paths. The probability of detection in the multi-path scenario can still be expressed by using the generalized Marcum-Q function, with the total signal power incorporating contributions from all paths:

$$\begin{aligned}P_d = Q_M\Bigg(\frac{\sqrt{2}|\alpha|^2 P_t}{\sigma_n}\Bigg|\boldsymbol{h}_{\mathrm{a,r}}\Bigg(\sum_{m=1}^{L_{\mathrm{t,a}}}\boldsymbol{h}_{\mathrm{t,a},m} \\ + \sum_{n=1}^{L_{\mathrm{s,a}}}\boldsymbol{h}_{\mathrm{s,a},n}\boldsymbol{\Psi}\sum_{k=1}^{L_{\mathrm{t,s}}}\boldsymbol{H}_{\mathrm{t,s},k}\Bigg)\Bigg|^2, \frac{\sqrt{2}}{\sigma_n}\gamma\Bigg),\end{aligned} \tag{44}$$

where it is worth noting that, since the LOS and NLOS paths may add destructively, the total received target power may decrease, leading to a lower detection probability compared to the single-path case.

Next, we evaluate the performance numerically. In our simulation, we consider a scenario with one LOS path and

two NLOS paths for each channel in the system, where the Rician factor is set to $K = 13.2$ dB according to [38]. For simplicity, RIS-CF is employed to determine the RIS beamformer due to its lower complexity. Figs. 5(a) and 5(b) depict the probability of detection P_d versus SNR for both the single-path and multi-path scenarios, comparing the RIS and non-RIS schemes in Case 1 (see Section V-A). It is observed that the theoretical results obtained from (44) align well with the simulation outcomes. Compared to the single-path case, the LOS-focused design with multi-path channels is unable to fully align the NLOS and LOS paths, resulting in some degradation in detection performance. Nevertheless, the RIS scheme still offers significant performance improvement over the non-RIS scheme, because the benefits offered by RIS outweigh the interference caused by the NLOS paths.

VI. Conclusion

In this paper, we examined a bistatic RF sensing system that employs an RIS to enhance target illumination. We derived a closed-form solution to the joint beamforming design problem for the RIS-assisted sensing system, which is computationally more efficient than the state-of-the-art manifold optimization approach. In addition, we provided an analytical and quantitative analysis of the system's target detection performance when either the TX or RIS faces obstruction. Our findings demonstrate that the RIS-assisted sensing system can significantly enhance detection performance, even in the presence of substantial channel estimation errors. Although the proposed beamforming scheme is focused on the LOS path, numerical results indicate that it outperforms conventional non-RIS schemes in wireless environments where the LOS path is typically stronger than the NLOS paths. In future work, we may explore the use of active RIS for RF sensing, which offers enhanced signal coverage, greater signal strength, and more flexible control [39]. However, it is important to note that passive RIS, with its advantages in energy efficiency and lower implementation costs, remains highly valuable for many applications.

References

[1] K.-P.-H. Thai, O. Rabaste, J. Bosse, D. Poullin, I. D. H. Senz, T. Letertre, and T. Chonavel, "Detectionlocalization algorithms in the around-the-corner radar problem," *IEEE Transactions on Aerospace and Electronic Systems*, vol. 55, no. 6, pp. 2658–2673, 2019.

[2] H. Li, F. Wang, C. Zeng, and M. A. Govoni, "Signal detection in distributed MIMO radar with non-orthogonal waveforms and sync errors," *IEEE Transactions on Signal Processing*, vol. 69, pp. 3671–3684, 2021.

[3] C. Pan, G. Zhou, K. Zhi, S. Hong, T. Wu, Y. Pan, H. Ren, M. Di Renzo, A. L. Swindlehurst, R. Zhang *et al.*, "An overview of signal processing techniques for RIS/IRS-aided wireless systems," *IEEE Journal of Selected Topics in Signal Processing*, vol. 16, no. 5, pp. 883–917, 2022.

[4] C. Pan, H. Ren, K. Wang, J. F. Kolb, M. Elkashlan, M. Chen, M. Di Renzo, Y. Hao, J. Wang, A. L. Swindlehurst, X. You, and L. Hanzo, "Reconfigurable intelligent surfaces for 6G systems: Principles, applications, and research directions," *IEEE Communications Magazine*, vol. 59, no. 6, pp. 14–20, 2021.

[5] P. Wang, J. Fang, X. Yuan, Z. Chen, and H. Li, "Intelligent reflecting surface-assisted millimeter wave communications: Joint active and passive precoding design," *IEEE Transactions on Vehicular Technology*, vol. 69, no. 12, pp. 14 960–14 973, 2020.

[6] Z. Lin, M. Lin, B. Champagne, W.-P. Zhu, and N. Al-Dhahir, "Secrecy-energy efficient hybrid beamforming for satellite-terrestrial integrated networks," *IEEE Transactions on Communications*, vol. 69, no. 9, pp. 6345–6360, 2021.

[7] Z. Lin, H. Niu, K. An, Y. Wang, G. Zheng, S. Chatzinotas, and Y. Hu, "Refracting RIS-aided hybrid satellite-terrestrial relay networks: Joint beamforming design and optimization," *IEEE Transactions on Aerospace and Electronic Systems*, vol. 58, no. 4, pp. 3717–3724, 2022.

[8] Z. Lin and et al., "Self-powered absorptive reconfigurable intelligent surfaces for securing satellite-terrestrial integrated networks," *China Communications*, vol. 21, no. 9, pp. 276–291, 2024.

[9] K. An, Y. Sun, Z. Lin, Y. Zhu, W. Ni, N. Al-Dhahir, K.-K. Wong, and D. Niyato, "Exploiting multi-layer refracting RIS-assisted receiver for HAP-SWIPT networks," *IEEE Transactions on Wireless Communications*, vol. 23, no. 10, pp. 12 638–12 657, 2024.

[10] A. Aubry, A. De Maio, and M. Rosamilia, "Reconfigurable intelligent surfaces for N-LOS radar surveillance," *IEEE Transactions on Vehicular Technology*, vol. 70, no. 10, pp. 10 735–10 749, 2021.

[11] S. Buzzi, E. Grossi, M. Lops, and L. Venturino, "Foundations of MIMO radar detection aided by reconfigurable intelligent surfaces," *IEEE Transactions on Signal Processing*, vol. 70, pp. 1749–1763, 2022.

[12] ——, "Radar target detection aided by reconfigurable intelligent surfaces," *IEEE Signal Processing Letters*, vol. 28, pp. 1315–1319, 2021.

[13] W. Lu, Q. Lin, N. Song, Q. Fang, X. Hua, and B. Deng, "Target detection in intelligent reflecting surface aided distributed MIMO radar systems," *IEEE Sensors Letters*, vol. 5, no. 3, pp. 1–4, 2021.

[14] Z. Xie, L. Wu, J. Zhu, M. Lops, X. Huang, and M. R. B. Shankar, "RIS-aided radar for target detection: Clutter region analysis and joint active-passive design," *IEEE Transactions on Signal Processing*, vol. 72, pp. 1706–1723, 2024.

[15] Z. Chen, J. Tang, L. Huang, Z.-Q. He, K.-K. Wong, and J. Wang, "Robust target positioning for reconfigurable intelligent surface assisted MIMO radar systems," *IEEE Transactions on Vehicular Technology*, 2023.

[16] Y. Liu, M. Ahmadi, J. Fuchs, and M. R. B. Shankar, "Time-code-spatial modulated IRS-aided radar localization in NLoS scenario," in *2023 IEEE Radar Conference (RadarConf23)*, 2023, pp. 1–5.

[17] E. Grossi, H. Taremizadeh, and L. Venturino, "Radar target detection and localization aided by an active reconfigurable intelligent surface," *IEEE Signal Processing Letters*, vol. 30, pp. 903–907, 2023.

[18] Z. Esmaeilbeig, K. V. Mishra, and M. Soltanalian, "IRS-aided radar: Enhanced target parameter estimation via intelligent reflecting surfaces," in *2022 IEEE 12th Sensor Array and Multichannel Signal Processing Workshop (SAM)*. IEEE, 2022, pp. 286–290.

[19] Z. Esmaeilbeig, A. Eamaz, K. V. Mishra, and M. Soltanalian, "Joint waveform and passive beamformer design in multi-IRS-aided radar," in *ICASSP 2023 - 2023 IEEE International Conference on Acoustics, Speech and Signal Processing (ICASSP)*, 2023, pp. 1–5.

[20] F. Wang, H. Li, and J. Fang, "Joint active and passive beamforming for IRS-assisted radar," *IEEE Signal Processing Letters*, vol. 29, pp. 349–353, 2021.

[21] R. Liu, M. Li, and Q. Liu, "Joint transmit waveform and reflection design for RIS-assisted MIMO radar systems," *IEEE Communications Letters*, vol. 27, no. 2, pp. 615–619, 2023.

[22] F. Wang, H. Li, and A. L. Swindlehurst, "Clutter suppression for target detection using hybrid reconfigurable intelligent surfaces," in *2023 IEEE Radar Conference (RadarConf23), May 1-5, 2023, San Antonio, Texas*, 2023, pp. 1–5.

[23] F. Wang, A. L. Swindlehurst, and H. Li, "Detection performance of RIS-Aided MIMO radar with asynchronous propagation," in *2023 IEEE International Workshop on Computational Advances in Multi-Sensor Adaptive Processing (CAMSAP 2023), DECEMBER 10-13, 2023, LOS SUEOS, COSTA RICA*, 2023.

[24] Y. He, Y. Cai, H. Mao, and G. Yu, "RIS-assisted communication radar coexistence: Joint beamforming design and analysis," *IEEE Journal on Selected Areas in Communications*, vol. 40, no. 7, pp. 2131–2145, 2022.

[25] M. Luan, B. Wang, Z. Chang, T. Hmlinen, and F. Hu, "Robust beamforming design for RIS-aided integrated sensing and communication system," *IEEE Transactions on Intelligent Transportation Systems*, vol. 24, no. 6, pp. 6227–6243, 2023.

[26] A. Bazzi and M. Chafii, "RIS-enabled passive radar towards target localization," *arXiv preprint arXiv:2210.11887*, 2022.

[27] C. Ozturk, M. F. Keskin, H. Wymeersch, and S. Gezici, "RIS-aided near-field localization under phase-dependent amplitude variations," *IEEE Transactions on Wireless Communications*, 2023.

[28] R. Liu, M. Li, H. Luo, Q. Liu, and A. L. Swindlehurst, "Integrated sensing and communication with reconfigurable intelligent surfaces:

Opportunities, applications, and future directions," *IEEE Wireless Communications*, vol. 30, no. 1, pp. 50–57, 2023.
[29] R. P. Sankar, S. P. Chepuri, and Y. C. Eldar, "Beamforming in integrated sensing and communication systems with reconfigurable intelligent surfaces," *IEEE Transactions on Wireless Communications*, 2023.
[30] K. Zhong, J. Hu, C. Pan, M. Deng, and J. Fang, "Joint waveform and beamforming design for RIS-aided ISAC systems," *IEEE Signal Processing Letters*, vol. 30, pp. 165–169, 2023.
[31] R. Liu, M. Li, Q. Liu, and A. L. Swindlehurst, "SNR/CRB-constrained joint beamforming and reflection designs for RIS-ISAC systems," *IEEE Transactions on Wireless Communications*, pp. 1–1, 2023.
[32] G. Cui, H. Li, and M. Rangaswamy, "MIMO radar waveform design with constant modulus and similarity constraints," *IEEE Transactions on Signal Processing*, vol. 62, no. 2, pp. 343–353, 2014.
[33] N. Boumal, B. Mishra, P.-A. Absil, and R. Sepulchre, "Manopt, a Matlab toolbox for optimization on manifolds," *Journal of Machine Learning Research*, vol. 15, no. 1, pp. 1455–1459, 2014.
[34] K. Alhujaili, V. Monga, and M. Rangaswamy, "Transmit MIMO radar beampattern design via optimization on the complex circle manifold," *IEEE Transactions on Signal Processing*, vol. 67, no. 13, pp. 3561–3575, 2019.
[35] P. Wang, J. Fang, H. Duan, and H. Li, "Compressed channel estimation for intelligent reflecting surface-assisted millimeter wave systems," *IEEE Signal Processing Letters*, vol. 27, pp. 905–909, 2020.
[36] O. El Ayach, S. Rajagopal, S. Abu-Surra, Z. Pi, and R. W. Heath, "Spatially sparse precoding in millimeter wave MIMO systems," *IEEE transactions on wireless communications*, vol. 13, no. 3, pp. 1499–1513, 2014.
[37] X. Gao, L. Dai, S. Han, I. Chih-Lin, and R. W. Heath, "Energy-efficient hybrid analog and digital precoding for mmwave MIMO systems with large antenna arrays," *IEEE Journal on Selected Areas in Communications*, vol. 34, no. 4, pp. 998–1009, 2016.
[38] Z. Muhi-Eldeen, L. Ivrissimtzis, and M. Al-Nuaimi, "Modelling and measurements of millimetre wavelength propagation in urban environments," *IET microwaves, antennas & propagation*, vol. 4, no. 9, pp. 1300–1309, 2010.
[39] Z. Yu, H. Ren, C. Pan, G. Zhou, B. Wang, M. Dong, and J. Wang, "Active RIS-aided ISAC systems: Beamforming design and performance analysis," *IEEE Transactions on Communications*, vol. 72, no. 3, pp. 1578–1595, 2024.

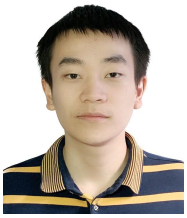

Cengcang Zeng received the B.S. degree from Nanjing University of Aeronautics and Astronautics, Nanjing, China in 2016 and the M.S. degree from Stevens Institute of Technology, Hoboken, NJ, USA in 2018, both in electrical engineering. He is currently pursuing the Ph.D. degree in electrical engineering at Stevens Institute of Technology, Hoboken, NJ, USA. His research interests include statistical signal processing and convex optimization, focusing on radar signal processing.

Hongbin Li (M'99-SM'08-F'19) received the B.S. and M.S. degrees from the University of Electronic Science and Technology of China, in 1991 and 1994, respectively, and the Ph.D. degree from the University of Florida, Gainesville, FL, in 1999, all in electrical engineering.

From July 1996 to May 1999, he was a Research Assistant in the Department of Electrical and Computer Engineering at the University of Florida. Since July 1999, he has been with the Department of Electrical and Computer Engineering, Stevens Institute of Technology, Hoboken, NJ, where he is currently the Charles and Rosanna Batchelor Memorial Chair Professor. He was a Summer Visiting Faculty Member at the Air Force Research Laboratory in the summers of 2003, 2004 and 2009. His general research interests include statistical signal processing, wireless communications, and radars.

Dr. Li received a number of awards including the IEEE Jack Neubauer Memorial Award in 2013, Master of Engineering (Honoris Causa) from Stevens Institute of Technology in 2024, Provost's Award for Research Excellence in 2019, Harvey N. Davis Teaching Award in 2003, and Jess H. Davis Memorial Research Award in 2001, and Sigma Xi Graduate Research Award from the University of Florida in 1999. He has been a member of the IEEE SPS Signal Processing Theory and Methods Technical Committee (TC) and the IEEE SPS Sensor Array and Multichannel TC, an Associate Editor for *Signal Processing* (Elsevier), *IEEE Transactions on Signal Processing*, *IEEE Signal Processing Letters*, and *IEEE Transactions on Wireless Communications*, as well as a Guest Editor for *IEEE Journal of Selected Topics in Signal Processing* and *EURASIP Journal on Applied Signal Processing*. He has been involved in various conference organization activities, including serving as a General Co-Chair for the 7th IEEE Sensor Array and Multichannel Signal Processing (SAM) Workshop, Hoboken, NJ, June 17-20, 2012. Dr. Li is a member of Tau Beta Pi and Phi Kappa Phi, and a fellow of the Asia-Pacific Artificial Intelligence Association (AAIA) and the International Artificial Intelligence Industry Alliance (AIIA).